Applications of Mathematics

Josef Málek; Kumbakonam R. Rajagopal; Petra Suková

Response of a class of mechanical oscillators described by a novel system of differential-algebraic equations

Applications of Mathematics, Vol. 61 (2016), No. 1, 79–102

Persistent URL: http://dml.cz/dmlcz/144813

61 (2016) APPLICATIONS OF MATHEMATICS No. 1, 79–102

RESPONSE OF A CLASS OF MECHANICAL OSCILLATORS DESCRIBED BY A NOVEL SYSTEM OF DIFFERENTIAL-ALGEBRAIC EQUATIONS

Josef Málek, Praha, Kumbakonam R. Rajagopal, College Station,
Petra Suková, Warsaw

(Received December 16, 2014)

Abstract. We study the vibration of lumped parameter systems whose constituents are described through novel constitutive relations, namely implicit relations between the forces acting on the system and appropriate kinematical variables such as the displacement and velocity of the constituent. In the classical approach constitutive expressions are provided for the force in terms of appropriate kinematical variables, which when substituted into the balance of linear momentum leads to a single governing ordinary differential equation for the system as a whole. However, in the case considered we obtain a system of equations: the balance of linear momentum, and the implicit constitutive relation for each constituent, that has to be solved simultaneously. From the mathematical perspective, we have to deal with a differential-algebraic system. We study the vibration of several specific systems using standard techniques such as Poincaré's surface of section, bifurcation diagrams, and Lyapunov exponents. We also perform recurrence analysis on the trajectories obtained.

Keywords: chaos; differential-algebraic system; Poincaré's sections; recurrence analysis; bifurcation diagram; implicit constitutive relations; Duffing oscillator; Bingham dashpot; rigid-elastic spring

MSC 2010: 34C28, 70K55, 34A09

1. Introduction

Mechanical oscillators consisting of springs and dashpots are usually described by

This work was initiated and mostly performed during the research stay of P. Suková at the Department of Mechanical Engineering at Texas A&M University. The research has been supported in part by GAUK-428011 and by DEC-2012-/05/E/ST9/03914 from the Polish National Science Center (P.S.), J. Málek acknowledges the support of the ERC-CZ project LL1202 financed by MŠMT (Ministry of Education, Youth and Sports of the Czech Republic).

constitutive relations for the forces in terms of the relevant kinematical variables which are then substituted into the balance of linear momentum for the lumped parameter system, leading to an ordinary differential equation for the displacement. If one considers a simple system as described by Fig. 1, the balance of linear momentum takes the form

$$m\ddot{x} = F_{\text{app}} - F_s - F_d, \tag{1.1}$$

where F_{app}, F_s and F_d represent the applied force, the force in the spring and the force in the dashpot, respectively, x is the displacement and m is the mass of the body, the dot denotes time derivatives. In what follows, we consider only problems and examples with $m = 1$ and the applied force in the form

$$F_{\text{app}} = A\cos\omega t. \tag{1.2}$$

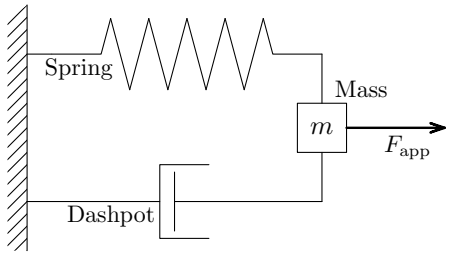

Figure 1. Oscillatory system with standard spring and dashpot.

The constitutive relations for the spring and the dashpot usually take the form

$$F_s = f(x), \tag{1.3}$$

$$F_d = g(\dot{x}), \tag{1.4}$$

and the system (1.1)–(1.4) is rendered determinate by providing the initial conditions

$$x(0) = x_0 \quad \text{and} \quad \dot{x}(0) = v_0. \tag{1.5}$$

When f and g are nonlinear functions, the system (1.1)–(1.5) leads to interesting problems and various nonlinear functions have been studied.

There are however many important physical problems wherein one cannot specify the force in the spring F_s or the dashpot F_d explicitly in terms of the displacement and velocity, respectively, as assumed in (1.3) and (1.4). A simple example where the spring force cannot be expressed explicitly in terms of the displacement is a system

comprising a rigid-elastic spring where the extension of the spring is possible only if the force F_s exceeds certain threshold. In such a situation, the force in the spring is not a function of the displacement, but the displacement is a function of the force F_s (see the graph on the left in Fig. 10). Similarly, a dashpot containing a Bingham fluid wherein one has to overcome a yield stress before the fluid starts flowing is a situation where one cannot express the friction force F_d as a function of the velocity (see the graph on the right in Fig. 13). One could yet choose to express the forces in terms of the kinematics, but in such a case one should interpret solutions as solutions to differential inclusions (see Filippov [9], [10]) and in some cases use complicated ideas such as "measure differential inclusions" (see Stewart [22] or Aubin and Cellina [1]) or multi-valued differential equations (see Deimling [7]). Such mathematical complications are avoided if one simply chooses to express the kinematical quantities in terms of the forces, namely

$$x = h(F_s), \quad \dot{x} = l(F_d). \tag{1.6}$$

Since the functions h and l may not be invertible, the system (1.6) cannot be inverted to yield (1.3) and (1.4). It is possible to have mechanical oscillatory systems which are far more complicated wherein the constituents of the system could be given by implicit equations of the form

$$f_1(x, F_s) = 0, \quad f_2(\dot{x}, F_d) = 0, \tag{1.7}$$

or even more general implicit relation of the form

$$f_1(x, \dot{x}, F_s, F_d) = 0, \quad f_2(x, \dot{x}, F_s, F_d) = 0. \tag{1.8}$$

Two further important examples immediately come to mind wherein the constitutive relationships of the form (1.3) and (1.4) are completely inadequate. The first is a dissipative mechanism which is not a viscous dashpot due to solid Coulomb friction. In this case, an equation of the form (1.4) will fail to capture the physics. Another interesting example is the system depicted in Fig. 2 that consists of a spring, dashpot, inextensible string and mass. We shall not discuss the above examples in detail as such a discussion can be found in [18] and [17]. Also, unilateral constraints as those mentioned above lead to problems that are best studied within the context of constitutive equations which take the form (1.7). In all these cases, one needs a more general structure for the constitutive relation, namely one needs to use a more general constitutive equation than that of the form (1.3) and (1.4).

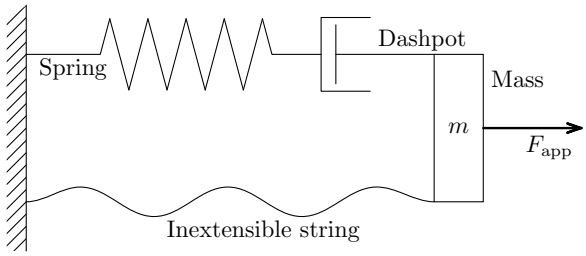

Figure 2. System that consists of a spring, dashpot, inextensible string and mass.

Zaki et al. [27] studied the response of a mass-spring system wherein the mass is hanging from a spring that is made of a nonlinear elastic solid. The mass can undergo radial motion and can also rotate about the point to which the spring is pinned. They showed that the motion of the system goes from a periodic attractor to a chaotic attractor, the route to chaos being a secondary Hopf bifurcation followed by torus-doubling bifurcation which eventually ends in torus breaking.

In this paper, we are interested in studying the response of several mechanical oscillatory systems, damped and undamped, whose components are given by constitutive equations of the form (1.6). We consider four specific examples. We will start by studying systems that are undamped. First of all, motivated by the classical Duffing oscillator described by

$$F_s = \beta_D x + \alpha_D x^3, \tag{1.9}$$

we study a nonstandard cubic oscillator given through

$$x = \alpha F_s + \beta F_s^3. \tag{1.10}$$

Then we investigate the behavior of the mass-spring system with the spring characterized by

$$x = \alpha(1 + \beta F_s^2)^{-1/3} F_s. \tag{1.11}$$

If

$$\alpha = \beta_D^{-1} > 0 \quad \text{and} \quad \beta = \alpha_D \beta_D^{-3} > 0, \tag{1.12}$$

then the spring responding according to (1.11) behaves asymptotically (for x and F_s small as well as for x and F_s large) as the classical Duffing oscillator (1.9) (see also Fig. 7). Thus, (1.11) provides an alternative to (1.9) if one is interested in capturing the response of the spring knowing its behavior only for x and F_s near zero and for

their large values. This is why we refer to the system responding by (1.11) the inverse Duffing oscillator. The Duffing oscillator with α_D and β_D having the opposite (non-physical within the setting considered) signs serves as a standard example of the simple evolutionary problem exhibiting chaotic motion with complicated bifurcation diagrams. For $\beta_D < 0$, the Duffing oscillator can be regarded as a model of a periodically forced steel beam which is acted upon by two magnets [15]. The remaining two examples studied in the paper, namely the linearly damped rigid-elastic spring (see Fig. 10) and the Bingham dashpot with linear spring (see Fig. 13), document that such chaotic behavior can be achieved for problems with physically relevant parameters as well.

We will use classical methods, such as Poincaré's surface of section, bifurcation diagrams and Lyapunov exponents [15] in this study. We solve the appropriate set of equations for each system using numerical implementation of the Runge-Kutta method of the 6th order with adaptive time step to achieve the desired accuracy. The output is the time series of the dependent variables $(x(t), \dot{x}(t), F_s(t), \dot{F}_s(t)$, etc.) with the chosen time step and the set of points forming Poincaré's surface of section. We will also perform two types of time series analysis, namely recurrence analysis, which lies in the statistical treatment of the moments when the trajectory returns to itself (for further details see [8] and [13]), and the computation of the weighted average of directional vectors (WADV), which involves comparing the direction of the trajectory at very near positions in the reconstructed phase space (see [11] and [21]). These methods for processing the time series were used recently also for studying chaos in geodesic motions ([23], [24], [12]). The implementation of the time series analysis is described in detail in the references listed above, particularly in [21], [25], [23], and [24]. Recurrence plots and quantifiers are computed using the software package described in [13] and available at [28].

It is important to recognize that contrary to the statements found in standard books on vibration such as Meirovitch [14], classical solutions do not exist when the dissipative mechanism is Coulomb friction, for which one may find a solution in the sense of Filippov (see [9], see also other approaches and references mentioned above). We do not investigate mathematical properties such as the appropriate concept of solution, its existence and qualitative behavior (stemming from the formulation (1.1)–(1.5)) in this study. We rather refer the interested reader to the results established in [16], [17]. Some cases such as Bingham fluids described using the setting of implicit constitutive relations or viscoelastic (Kelvin-Voigt) vibrating bodies have been analyzed even for three-dimensional bodies (large data), the existence of weak solutions has been established in [2], [3], and [4].

2. A spring with a non-standard cubic constitutive relation

We first study the problem wherein we have a very simple system, which we refer to as the inverse cubic constitutive relation for the spring, that is a spring defined through

$$x = \alpha F_s + \beta F_s^3, \tag{2.1}$$

where α and β are constant and

$$F_d = 0. \tag{2.2}$$

When α and β are positive, x defined through (2.1) is a monotonically increasing function (see Fig. 3) and hence one can invert the expression (2.1) and express the force in terms of the displacement and we will recover the classical procedure. While in principle the expression (2.1) can be inverted, as we are dealing with a cubic equation in F_s, we cannot obtain a simple explicit expression for F_s. On the other hand, with (2.1) we have a simple explicit expression for the displacement in terms of the spring force F_s. If α and β have opposite signs, such an inversion may not be possible. However, such a situation is not physically meaningful with regard to mass-spring-dashpot systems. We go ahead and consider the problem as it is very useful from the pedagogical point of view to introduce one to the notion of chaotic motion that arises as the solution to some differential equations (see [15]).

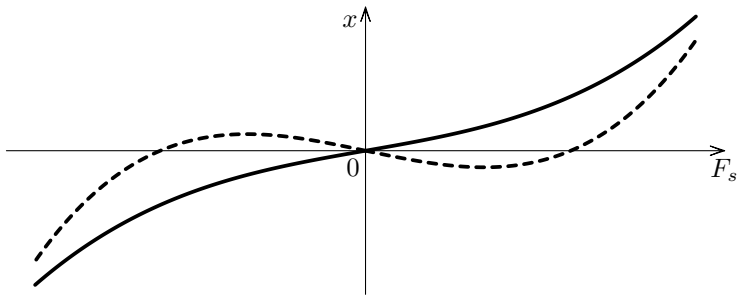

Figure 3. Relation between displacement and force for spring with a non-standard cubic constitutive relation with $\alpha > 0$, $\beta > 0$ (solid line) and $\alpha < 0$, $\beta > 0$ (dashed line).

In this case the problem reduces to

$$m(\alpha + 3\beta F_s^2)\ddot{F}_s + 6\beta m F_s \dot{F}_s^2 + F_s = F_{\text{app}}. \tag{2.3}$$

Since for non-negative α and β fulfilling $\alpha^2+\beta^2 \neq 0$, the equation (2.1) is invertible, it is appropriate to replace the initial conditions (1.5) by

$$F_s(0) = F_0, \quad \dot{F}_s(0) = \frac{1}{\alpha} v_0. \tag{2.4}$$

In Fig. 4, the force in the spring F_s is plotted as a function of time for specific values of α, β, ω and A and two different sets of initial conditions. In the next rows the respective Poincaré's surfaces, the recurrence plots and the WADV's[1] are given. Regular motion is seen in these plots, which means closed curves in the surface of section, long diagonal lines in the recurrence plot, and values close to $\Lambda = 1$ even for large time delays Δt for WADV. The latter reflects the fact that for regular motion the deterministic connection between the past and future of the orbit is strong during long periods of time and the evolution of the trajectory does not strongly depend on the initial conditions, which is an intrinsic feature of chaotic dynamics.

For the same parameters Poincaré's surface in the phase space is depicted in the first row of plots in Fig. 5 for a lot of trajectories with different initial conditions and it indicates regular motion. The zoom of the plot shows the primary island and the embedded islands with higher period. Similarly, Poincaré's surfaces for other sets of parameters are given in the second and third rows in Fig. 5 and they also indicate that the motion is regular, even for the case with negative α. We were unable to find chaotic motion, but since we have only tried specific choices for α, β, A, and ω, we cannot conclude that chaotic motion is not possible in such systems.

3. Inverse Duffing oscillator

A classic example of a system exhibiting chaotic behaviour for a certain subset of parameters is the well-known Generalized Duffing oscillator [15], [26], depicted in Fig. 6. The dynamics is governed by the equation

$$\ddot{x} + \delta_D \dot{x} + \beta_D x + \alpha_D x^3 = A \cos \omega t, \tag{3.1}$$

therefore, $F_s = \beta_D x + \alpha_D x^3$, $F_d = \delta_D \dot{x}$, and $F_{\text{app}} = A \cos \omega t$. The chaotic regime occurs in the generalized case, hence for $\beta_D < 0$. An example of such behaviour is illustrated in Fig. 8.

[1] The weighted average of directional vectors is defined as $\Lambda(\Delta t) = \langle ((V_j(\Delta t))^2 - (\overline{R}^d_{n_j})^2)/(1-(\overline{R}^d_{n_j})^2) \rangle$, where $V_j(\Delta t)$ is the length of the directional vector inside the j-th box in the phase space reconstructed with the delay technique with the time delay Δt normalized to n_j passages of the trajectory through that particular box, and $\overline{R}^d_{n_j}$ is the average displacement per step for random walk of length n_j in the d-dimensional space. See the details about the procedure and its numerical implementation in [21].

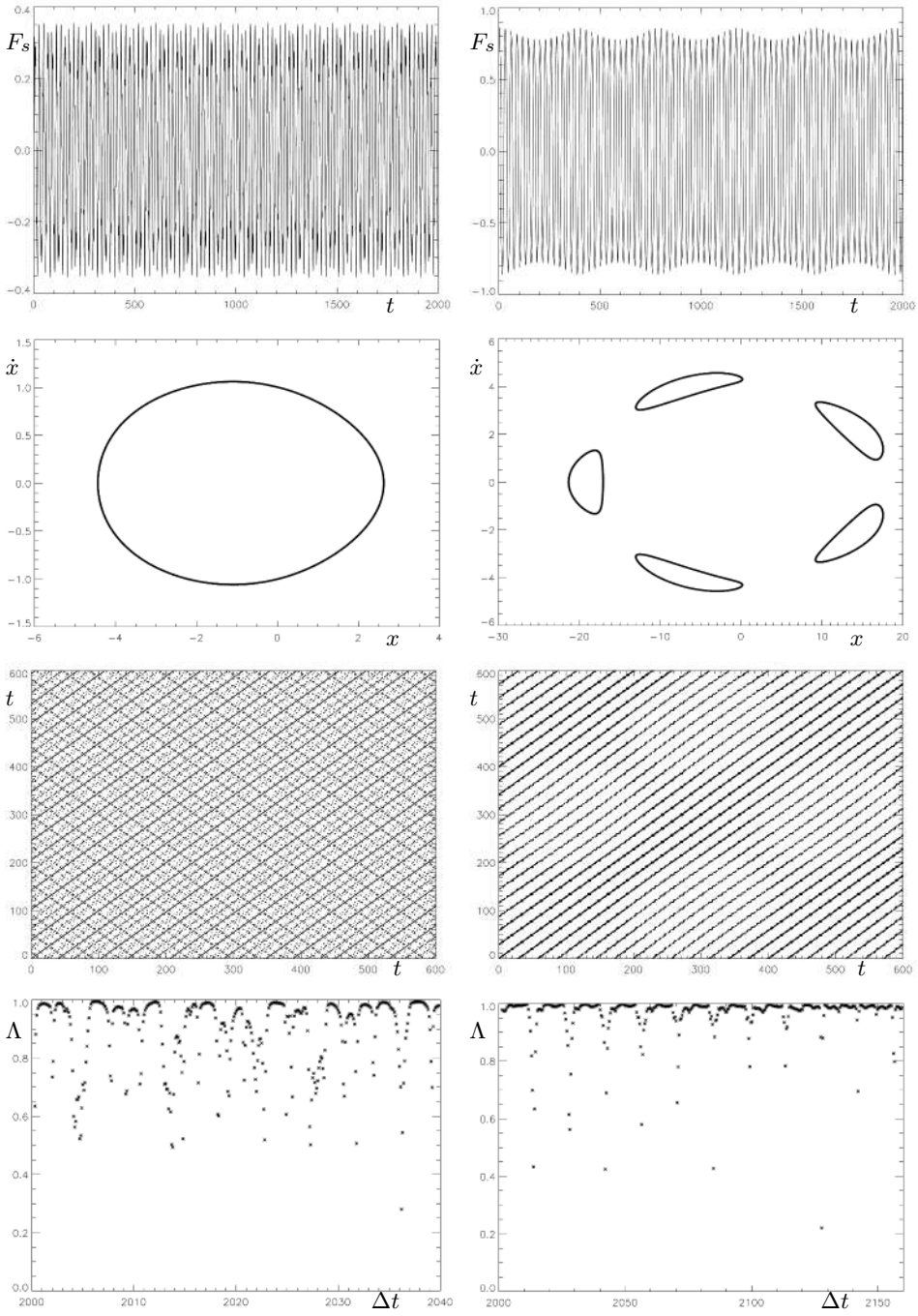

Figure 4. Non-standard cubic spring: $\alpha = 10$, $\beta = 20$, $A = 1.1$, $\omega = 1.1$, first column: $F_s(0) = -0.1$, $\dot{F}_s(0) = 0.1$, second column: $F_s(0) = 0.76$, $\dot{F}_s(0) = 0.05$.

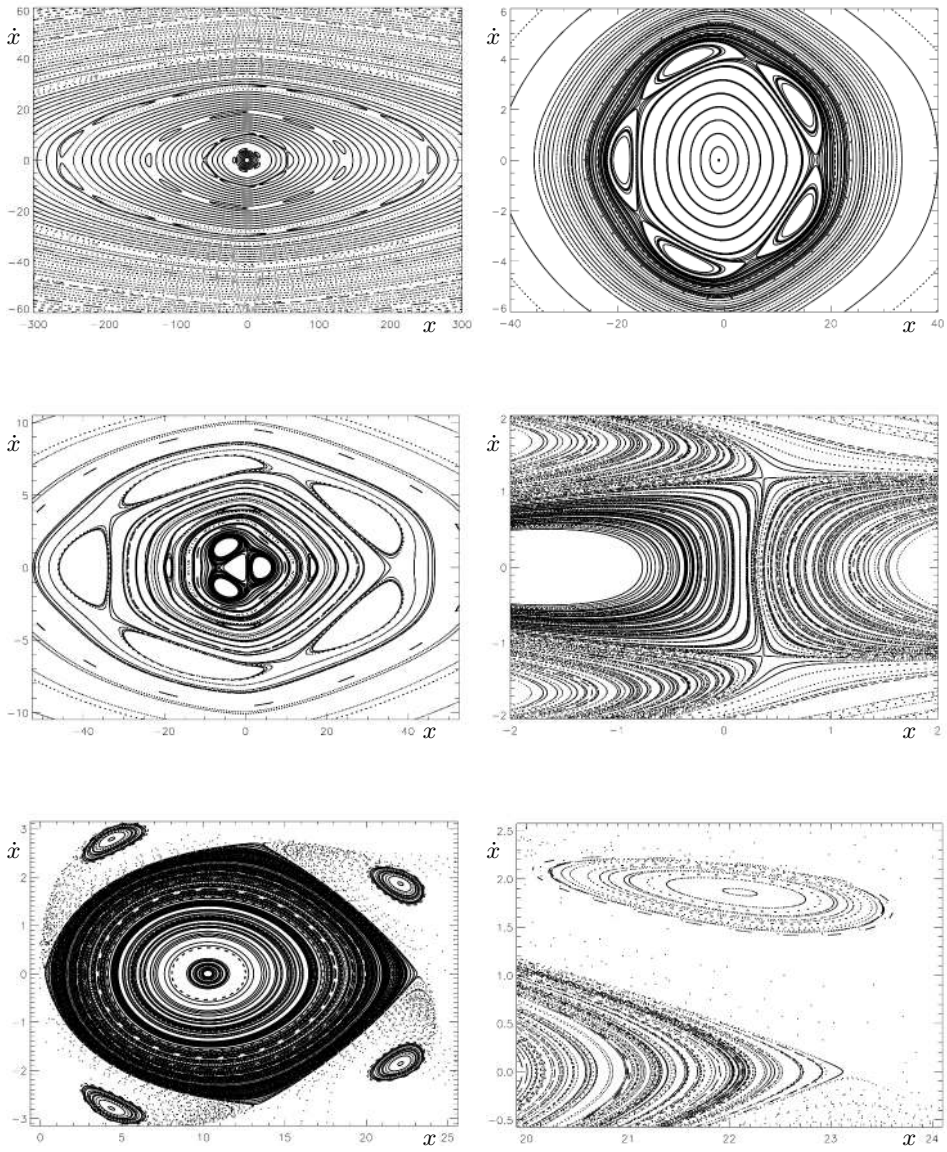

Figure 5. Non-standard cubic spring—Poincaré's surface of section depicting part of the phase space and the zoom of this plot on the right. We can see regular motion, the most important primary regular island and embedded islands with higher period.
First row: $\alpha = 10$, $\beta = 20$, $A = 1.1$, $\omega = 1.1$,
second row: $\alpha = 7.3$, $\beta = 33.7$, $A = 1.3$, $\omega = 0.85$,
third row: $\alpha = -0.6$, $\beta = 1.5$, $A = 0.5$, $\omega = 1.0$.

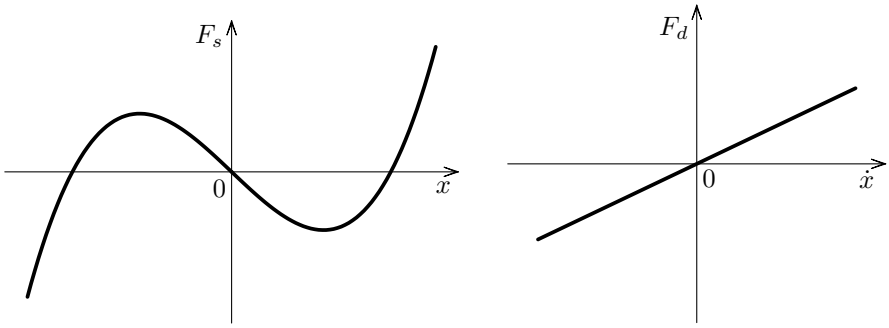

Figure 6. Relation between forces and displacement for Generalized Duffing oscillator with $\alpha_D > 0$, $\beta_D < 0$.

We can construct an analogue to the Duffing oscillator, which is constitutively described by the equations (1.1), (1.5), and (1.6) with

$$x = \alpha(1 + \beta F_s^2)^{-1/3} F_s, \quad \dot{x} = \gamma F_d. \tag{3.2}$$

This system, which we shall call the inverse Duffing oscillator (see Fig. 7), shows the same asymptotic behaviour as the Duffing oscillator with the following substitution of the parameters: $\alpha = \beta_D^{-1}$ by comparing the formulas for x and F_s near zero, $\beta = \alpha_D \alpha^3 = \alpha_D \beta_D^{-3}$ by comparing the formulas for x and F_s large; and $\gamma = \delta_D^{-1}$. However, we cannot directly compare the results with the Generalized Duffing oscillator depicted in Fig. 8, because for the corresponding parameters ($\alpha = -1$, $\beta = -1$, $\gamma = 2$) and high enough amplitude A the bracket in equation (3.2) becomes eventually equal to zero. Also the case with $\alpha < 0$ is not physically relevant in our setting, making the force in spring acting in the same direction as the displacement until the bracket reaches zero. We will study the dynamics of this system for $\alpha > 0$ and $\beta > 0$.

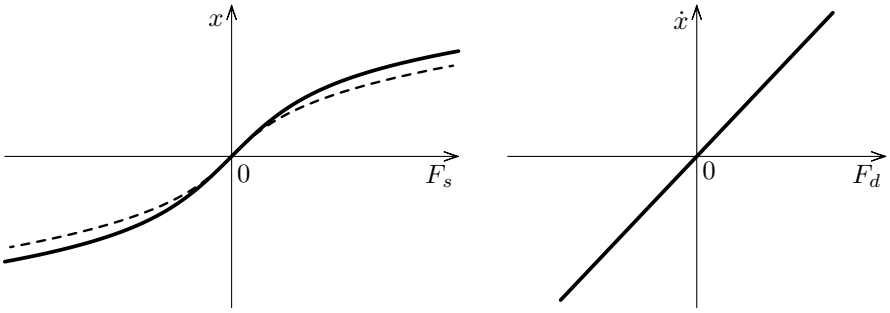

Figure 7. Relation between forces and displacement for inverse Duffing oscillator for $\alpha > 0$, $\beta > 0$ (solid line) and standard Duffing oscillator with the corresponding parameters $\alpha_D > 0$, $\beta_D > 0$ satisfying (1.12) (dashed line).

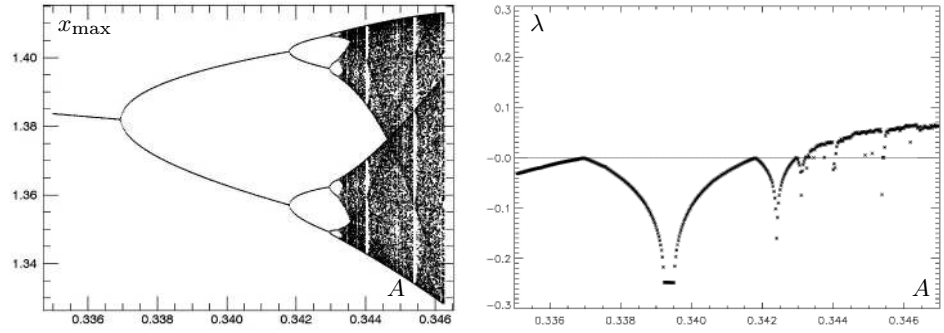

Figure 8. Maxima of $x(t)$ (bifurcation diagram – left) and the maximal Lyapunov exponent obtained by the two-particle method (right) for the Generalized Duffing oscillator with $\alpha_D = 1$, $\beta_D = -1$, $\delta_D = 0.5$, $\omega = 0.9$ versus changing amplitude of the driving force A.

The relations (3.2) immediately imply that

$$F_d = \frac{\dot{x}}{\gamma} = \frac{1}{\gamma}\Big(\alpha(1+\beta F_s^2)^{-1/3}\dot{F}_s - \frac{1}{3}\alpha(1+\beta F_s^2)^{-4/3}2\beta F_s^2\dot{F}_s\Big). \tag{3.3}$$

After performing another differentiation of equation (3.2) we obtain the acceleration in the form

$$\begin{aligned}\ddot{x} = {} & \alpha(1+\beta F_s^2)^{-1/3}\ddot{F}_s\Big(1 - \frac{2\beta F_s^2}{3(1+\beta F_s^2)}\Big) \\ & + \frac{2\alpha\beta}{3}(1+\beta F_s^2)^{-4/3}F_s(\dot{F}_s)^2\Big\{\frac{8\beta F_s^2}{3(1+\beta F_s^2)} - 3\Big\}.\end{aligned} \tag{3.4}$$

Hence, equation (1.1) could be written in the form

$$\begin{aligned}\ddot{F}_s = {} & \frac{(1+\beta F_s^2)^{1/3}(F_{\rm app} - F_s) - \alpha\dot{F}_s/\gamma}{\alpha m\big(1 - 2\beta F_s^2/3(1+\beta F_s^2)\big)} \\ & + \frac{2\alpha\beta(3(1+\beta F_s^2))^{-1}F_s\dot{F}_s\big(F_s/\gamma - m\dot{F}_s\big(8\beta F_s^2/3(1+\beta F_s^2) - 3\big)\big)}{\alpha m\big(1 - 2\beta F_s^2/3(1+\beta F_s^2)\big)}\end{aligned} \tag{3.5}$$

with initial conditions given by $F_s(0) = F_0$ and $\dot{F}_s(0) = F_1$.

The orbits of the dissipating system settle down after some time into the attractor. For regular motion, Poincaré's surface of section for the attractor consists only of few distinct points, and the chaotic attractor has non-integer dimension and yields fractal structure in the surface of the section. Contrary to conservative systems, in dissipative systems we can study the bifurcation diagram, where we plot all local maxima of $x(t)$ or $F_s(t)$ against a changing parameter of the system. In practise,

we evolve the orbit for some transient time to wait until the trajectory converges into the attractor, and then we start to record the positions of local maxima. In order to have the complete bifurcation diagram, we need to cover initial conditions for all existing attractors for the given value of the parameter. In these diagrams the sudden changes (called bifurcations) of the nature of the orbit at a specific value of the parameter can be seen as well as the regular and the chaotic windows. The bifurcation diagram for the Generalized Duffing oscillator is well known, we give one example in Fig. 8. Similar diagrams for the inverse Duffing oscillator which we have obtained show no bifurcations, but only regular motion (for both α and β positive); an example is given in Fig. 9.

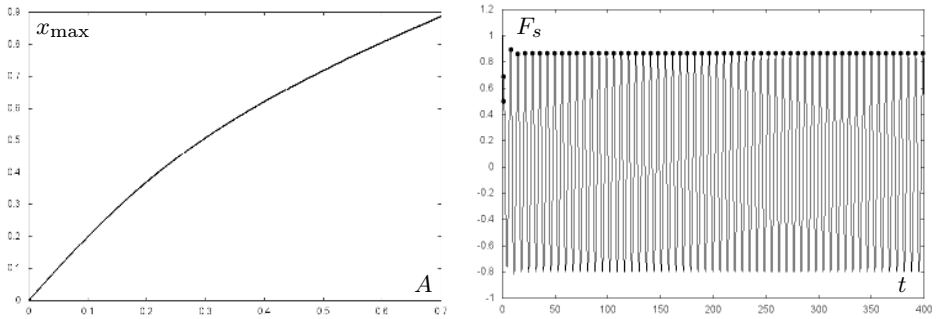

Figure 9. Maxima of $x(t)$ versus A for inverse Duffing oscillator with $\alpha = 1.0$, $\beta = 1.0$, $\gamma = 2.0$, and $\omega = 0.9$. In the right plot $F_s(t)$ for the particular trajectory with $A = 0.5$ is given. The maxima of $F_s(t)$ are labelled as points.

4. Rigid-elastic spring with linear dashpot

We will continue our study of non-standard dissipative systems with the rigid-elastic spring combined with linear dashpot, as is indicated in Fig. 10. The deflection of the spring is given by the relation (1.6), where

$$x = h(F_s) = \begin{cases} 0, & |F_s| \leqslant \delta, \\ \beta(F_s - \delta), & F_s > \delta, \\ \beta(F_s + \delta), & F_s < -\delta, \end{cases} \tag{4.1}$$

and the velocity is given by the force in the dashpot as

$$\dot{x} = \alpha F_d. \tag{4.2}$$

Equation (4.1) is non-invertible, thus F_s cannot be written in terms of x, but we can derive equations which hold for $|F_s| < \delta$ and for $|F_s| > \delta$. First we compute the

derivative of the relation (4.1):

$$\frac{\mathrm{d}h(F_s)}{\mathrm{d}F_s} = \begin{cases} 0, & |F_s| < \delta, \\ \beta, & |F_s| > \delta, \end{cases} \tag{4.3}$$

which holds everywhere except the points $|F_s| = \delta$.

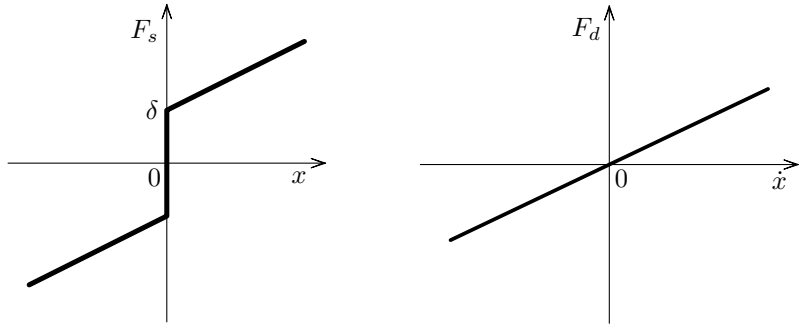

Figure 10. Relation between forces and displacement for the rigid-elastic spring with linear dashpot.

Now we proceed to study the response of the system separately in the two regions:
▷ $|F_s| < \delta$: From (4.1) the deflection of the spring is $x = 0$, which leads to $\dot{x} = 0$ and $\ddot{x} = 0$. The spring is at rest, therefore the force in the dashpot is also zero and from the equation of motion (1.1) we get a relation between the force in the spring and the applied force in the simple form

$$F_s(t) = F_{\mathrm{app}}(t). \tag{4.4}$$

Until the force in the spring reaches the threshold value δ again, the system is at rest.
▷ $|F_s| > \delta$:
We invert the relation (4.2) and get the force in the dashpot in terms of the velocity. Then using (4.3) and $\dot{x} = (\mathrm{d}h/\mathrm{d}F_s)\dot{F}_s$ we link the force in the dashpot and the force in the spring:

$$F_d = \frac{\dot{x}}{\alpha} = \frac{\beta}{\alpha}\dot{F}_s. \tag{4.5}$$

The acceleration is given by $\ddot{x} = (\mathrm{d}^2h/\mathrm{d}{F_s}^2)\dot{F}_s + (\mathrm{d}h/\mathrm{d}F_s)\ddot{F}_s$ and by differentiating (4.3) the term $\mathrm{d}^2h/\mathrm{d}{F_s}^2$ drops out. Next we obtain the second derivative of x in

terms of F_s, hence we are able to rewrite the equation of motion (1.1) in the form of a differential equation for F_s:

$$\ddot{x}(t) = \beta \ddot{F}_s(t), \tag{4.6}$$

$$\ddot{F}_s(t) = \frac{F_{\mathrm{app}}(t) - F_s(t) - \frac{\beta}{\alpha}\dot{F}_s(t)}{m\beta}. \tag{4.7}$$

We solve this set of equations using the Runge-Kutta method of the 6th order with adaptive time step (using equations (4.4) and (4.7) for $|F_s| < \delta$ and $|F_s| > \delta$, respectively) with the initial conditions $F_s(0)$ $(= x_0/\beta + \mathrm{sign}(F_s(0))\delta$ for $|F_s(0)| > \delta)$ and $\dot{F}_s(0)$ $(= (\alpha/\beta)F_d(0) = v_0/\beta$ for $|F_s(0)| > \delta)$. Thus we obtain $F_s(t)$ and $\dot{F}_s(t)$ from which we are able to compute $x(t)$ and $\dot{x}(t)$. Providing initial conditions in the form (1.5) is not appropriate for the multi-valued mapping from x to F_s in the case of a rigid-elastic spring (see Fig. 10) or from $\dot{x}$ to F_d in the case of a Bingham fluid in Section 5 (see Fig. 13).

In Fig. 11 bifurcation diagrams against changing amplitude A of the applied force (1.2) are given. In this system, we have chaotic behaviour for various values of the parameters. In the zoom of the bifurcation diagram, structures very similar to the bifurcation diagram of the Generalized Duffing oscillator (Fig. 8) can be seen, which is a typical demonstration of period-doubling bifurcation leading to chaotic motion.

For obtaining Lyapunov exponents we adopt the two-particle approach, in which the maximal Lyapunov exponent λ (mLE) is given by

$$\lambda = \lim_{t\to\infty} \frac{1}{t} \ln \frac{|\xi(t)|}{|\xi(0)|}, \tag{4.8}$$

where $\xi(t) = \mathbf{y} - \mathbf{y}^{\mathrm{sh}}$ is the deviation vector between the trajectory of the main particle described by the phase space vector $\mathbf{y} := (x, \dot{x})$ and its shadow, whose initial conditions differ slightly from the main particle, with the phase space vector $\mathbf{y}^{\mathrm{sh}}$. In our system the question is if we should compute the deviation vector as $[F_s(t) - F_s^{\mathrm{sh}}(t), \dot{F}_s(t) - \dot{F}_s^{\mathrm{sh}}(t)]$ or $[x(t) - x^{\mathrm{sh}}(t), \dot{x}(t) - \dot{x}^{\mathrm{sh}}(t)]$. On the first sight we would choose the norm in the physical phase-space $[x(t) - x^{\mathrm{sh}}(t), \dot{x}(t) - \dot{x}^{\mathrm{sh}}(t)]$. But these physical coordinates $x(t), \dot{x}(t)$ are not coordinates that fully describe the system, because for all $F_s(t) < \delta$, $x = 0$ and $\dot{x} = 0$, but the trajectory is not given uniquely and could be different with different F_s and $\dot{F}_s$. Also the renormalization in the context of the physical coordinates is not possible, because the relation (1.6) is non-invertible, so we cannot set the value of x and $\dot{x}$ and compute the corresponding $F_s, \dot{F}_s$ during the renormalization process. Therefore, we have chosen to compute the deviation vector as $\xi(t) = [F_s(t) - F_s^{\mathrm{sh}}(t), \dot{F}_s(t) - \dot{F}_s^{\mathrm{sh}}(t)]$.

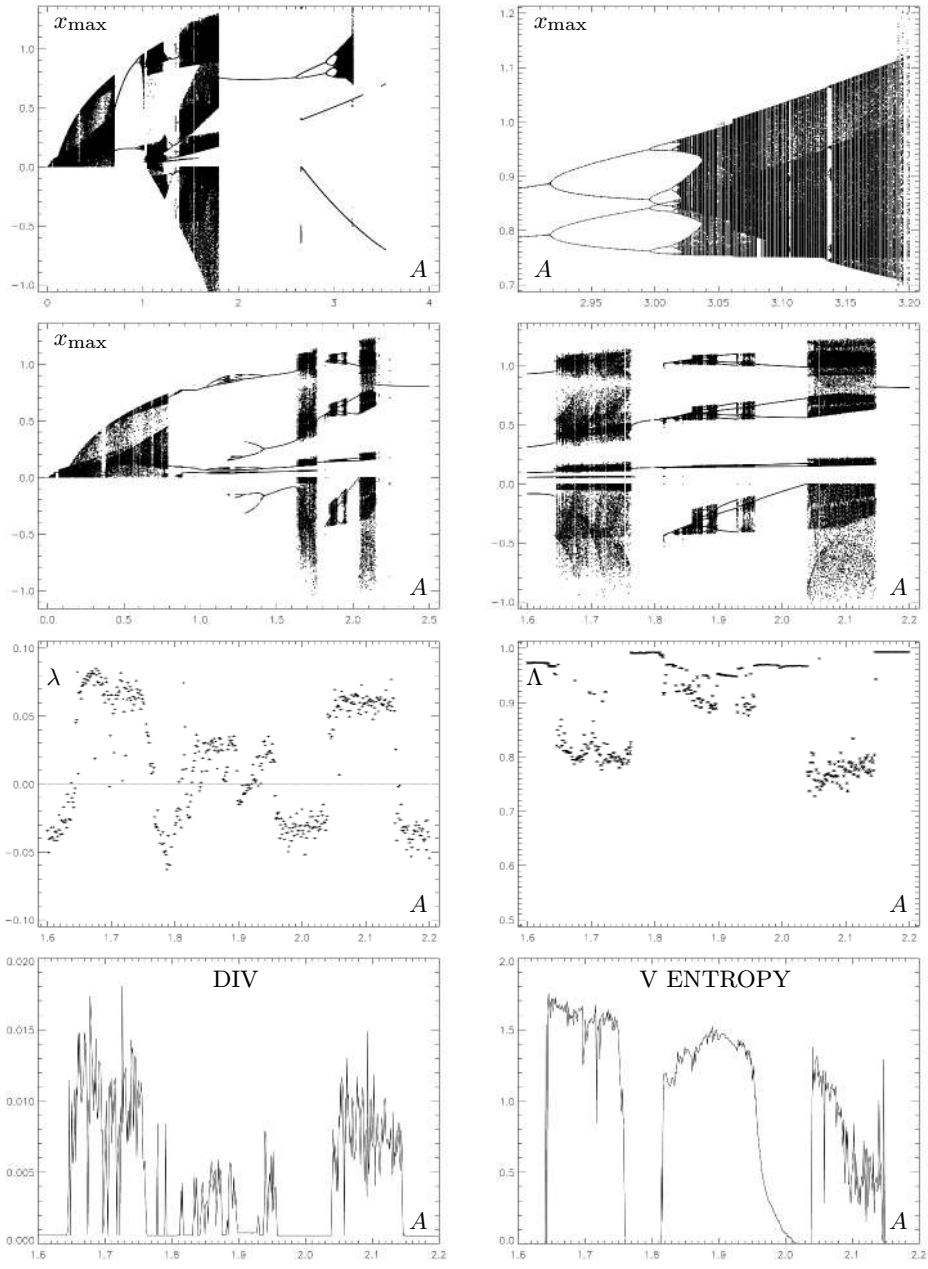

Figure 11. Rigid-elastic spring: first row: $\alpha = 0.8$, $\beta = 1.5$, $\delta = 0.8$, $\omega = 1.0$, bifurcation diagram and its zoom, next rows: $\alpha = 0.6$, $\beta = 1.5$, $\delta = 0.9$, $\omega = 1.0$, bifurcation diagram and its zoom, Lyapunov exponents and WADV, the recurrence quantifiers DIV and V ENTROPY for the zoomed window.

In Fig. 11 we plot the time-dependent mLE $\lambda(t_{\max})$, which instead of computing the limit in the relation (4.8) is the value attained after the total time of computation $t_{\max}$. In the regular region, this value is less than zero, because our system is dissipative, in the chaotic domain $\lambda(t_{\max}) > 0$.

Similarly, for the recurrence analysis and the computation of WADV we use the time series $F_s(t)$ instead of $x(t)$. These two methods are based on the recurrence of the system in the phase space and therefore if one uses $x(t)$ the results are marred by the degeneracy of the system at the point $[x(0), \dot{x}(0)]$. On the other hand, when using the coordinates $[F_s, \dot{F}_s]$ both these methods work perfectly. The WADV together with the recurrence quantifiers DIV and V ENTROPY (two quantifiers based on the statistical elaboration of the recurrence matrix as defined in [13]; DIV quantifier is given by the inverse of the longest diagonal line and V ENTROPY is the Shannon entropy of the vertical line length distribution) are given in the remaining plots in Fig. 11. In the chaotic regime the value of WADV (Λ) drops down significantly, which is due to the fact that the system is sensitive to initial conditions and therefore the phase space orbit can pass through one box in the phase space repeatedly with considerably different directions. On the other hand, the values of DIV, which can give a very rough estimate of the value of mLE, and of V ENTROPY, related to the appearance of vertical lines, go up for chaotic orbits.

For a certain range of amplitudes A there exist more than one attractor in the phase space, in our case for the same parameters for which the former analysis was done we have two different attractors. In Fig. 12 we plot $x(t)$ for those attractors ($A = 1.2$) and we mark the maxima with dots. The set of initial conditions which lead to one specific attractor is called the basin of attraction. We can map the phase space by computing many trajectories with initial conditions spread on a grid and label the points according to which basin they belong. Since we have two different attractors, we plot the initial condition with a black dot when it belongs to the basin of the first attractor while we do not plot a dot for the second. Examples of such maps for two different amplitudes are given in Fig. 12, where a complicated structure of the two sets can be seen, which is typical for chaotic systems and which indicates the non-integer dimension of these sets.

5. Bingham fluid

We complete our exploration of non-standard oscillating systems with a dashpot wherein the fluid is a Bingham fluid. This material does not flow unless a certain threshold in the force is reached in the dashpot, and when F_d is above a given threshold δ the viscous and elastic response is linear, see Fig. 13. Thus, the functions (1.6)

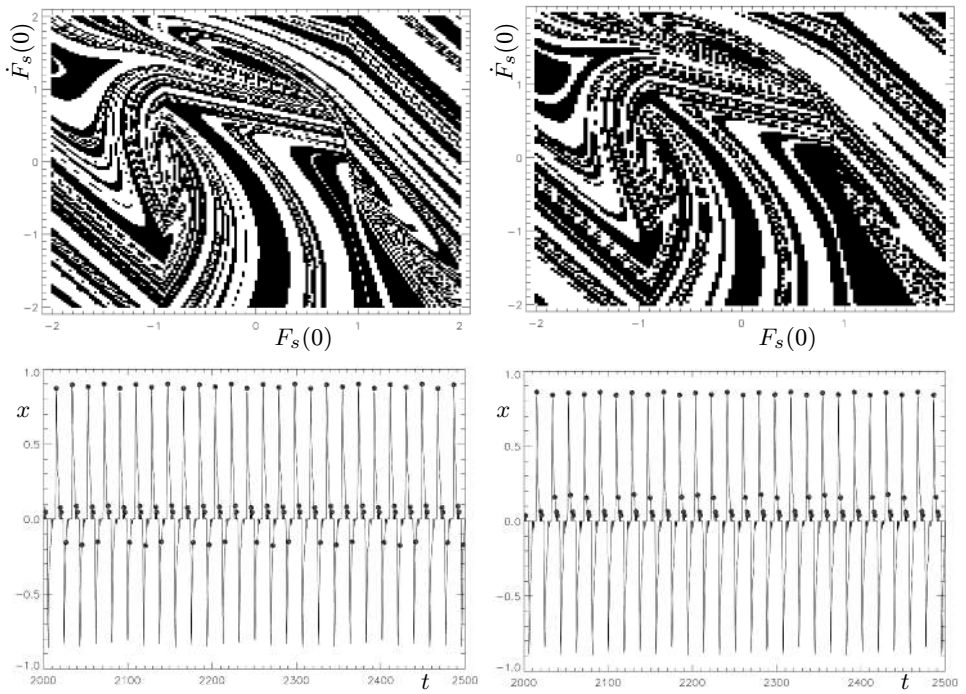

Figure 12. Rigid-elastic spring: $\alpha = 0.6$, $\beta = 1.5$, $\delta = 0.9$, $\omega = 1.0$, map of basins of two different attractors for the amplitude $A = 1.2$ (left) and $A = 1.3$ (right) in the first row, the course of $x(t)$ for the two attractors for $A = 1.2$ in the second row.

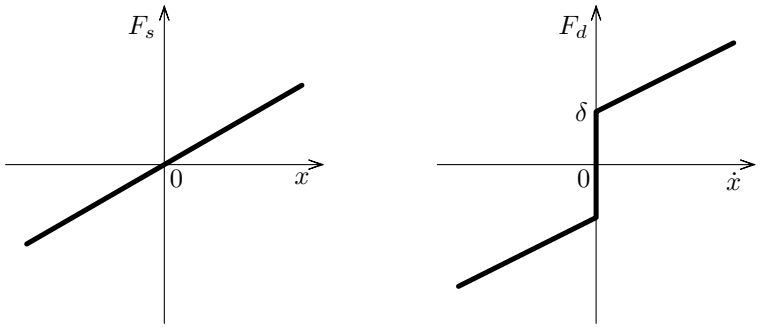

Figure 13. Relation between forces and displacement for a Bingham fluid.

have the form

$$x = \alpha F_s, \tag{5.1}$$

$$\dot{x} = g(F_d) = \begin{cases} 0, & |F_d| \leqslant \delta, \\ \beta(F_d - \delta), & F_d > \delta, \\ \beta(F_d + \delta), & F_d < -\delta, \end{cases} \tag{5.2}$$

which is an analogue of the rigid-elastic spring discussed in the previous section. We will now proceed to obtain the differential equation for our system. First we differentiate and invert (5.1) to obtain expressions for the time derivative of F_s:

$$\dot{x} = \alpha \dot{F_s} \Rightarrow \dot{F}_s = \frac{\dot{x}}{\alpha}. \tag{5.3}$$

Further we differentiate the equation of motion (1.1)

$$m\ddot{x} = F_{\text{app}} - F_s - F_d \tag{5.4}$$

to obtain

$$m\dddot{x} = \dot{F}_{\text{app}} - \dot{F}_s - \dot{F}_d. \tag{5.5}$$

We proceed to study the two regions separately.
▷ $|F_d| < \delta$: For forces below the value of the threshold, the velocity of the fluid is zero $\dot{x} = 0$, therefore the deflection $x = \text{const}$ and also $F_s = \text{const}$. From equation (5.5) we get the relation

$$\dot{F}_{\text{app}}(t) = \dot{F}_d(t). \tag{5.6}$$

▷ $|F_d| > \delta$: Differentiating (5.2) we express the time derivatives of x in terms of F_d:

$$\ddot{x} = \beta \dot{F}_d, \quad \dddot{x} = \beta \ddot{F}_d. \tag{5.7}$$

Using (5.3) and (5.7) from (5.5) we get a differential equation for F_d,

$$m\beta \ddot{F}_d = \dot{F}_{\text{app}} - \frac{\beta}{\alpha}(F_d - \text{sign}(F_d)\delta) - \dot{F}_d. \tag{5.8}$$

The deflection of the spring is then given by the integral

$$x(t) = \int_{s=0}^{t} g(F_d(s))\mathrm{d}s + x_0. \tag{5.9}$$

Thus, we compute a second order differential equation for F_d and we insert initial conditions $F_d(0)$ and $\dot{F}_d(0)$. They are related to the initial conditions $F_s(0)$ and $F_d(0)$ in the following way:

$$\dot{F}_d(0) = \frac{F_{\mathrm{app}}(0) - F_s(0) - F_d(0)}{m\beta}, \quad F_d(0) > \delta. \tag{5.10}$$

In Fig. 14 the bifurcation diagram (computed from $F_d(t)$) and its successive zooms are plotted. We can see the period-doubling bifurcations leading to chaotic regions, which end in regular windows with higher period. This pattern repeats within shorter and shorter amplitude periods, the regular and chaotic windows are shorter and shorter, therefore they are not visible in the big bifurcation diagram due to the sampling, but they appear after zooming. Examples of position of maxima of two trajectories, one belonging into the regular window and the other one from the chaotic region, are provided in Fig. 15.

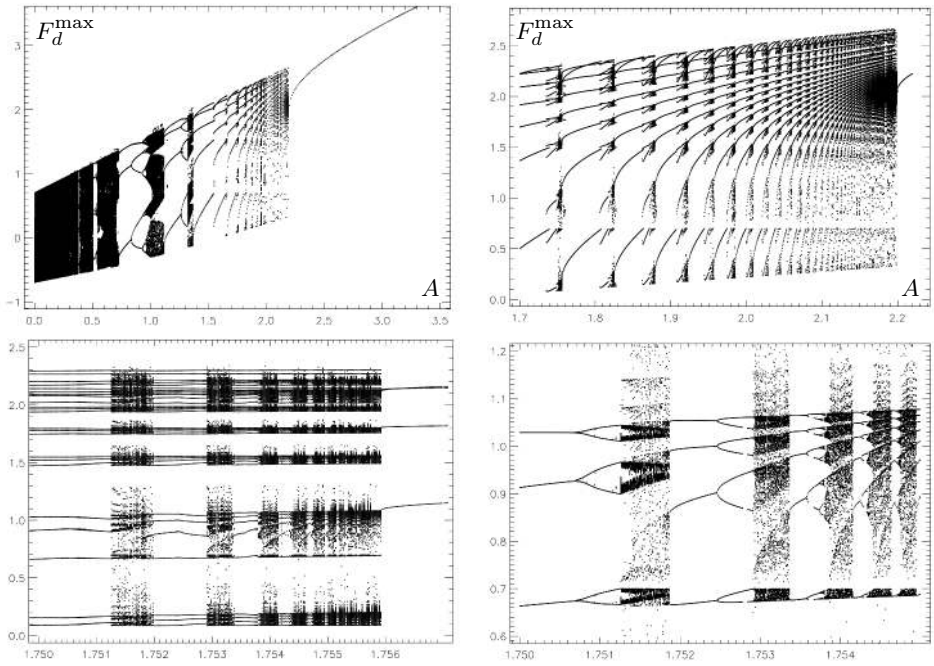

Figure 14. Bingham fluid: $\alpha = 0.6$, $\beta = 1.5$, $\delta = 0.7$, $\omega = 1.0$. Bifurcation diagram of the system (maxima of F_d) versus the changing amplitude of the driving force A and zoomed slices of it.

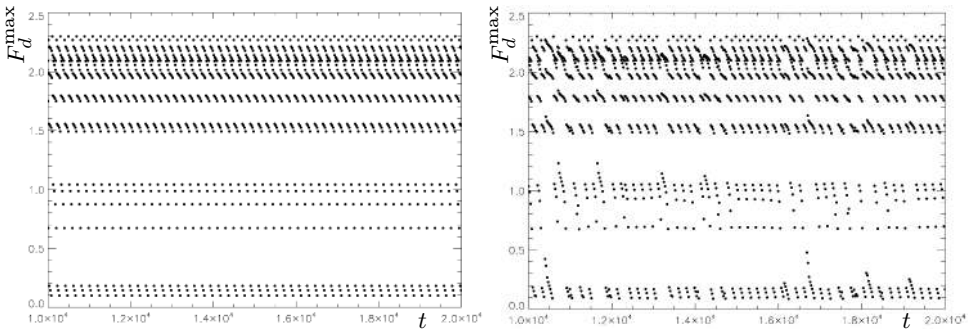

Figure 15. Bingham fluid: $\alpha = 0.6$, $\beta = 1.5$, $\delta = 0.7$, $\omega = 1.0$, maxima of $F_d(t)$ of the trajectories with high period, which exist for the amplitude $A = 1.7527$ (left) in the regular window and $A = 1.7532$ (right) in the chaotic region. These orbits belong to the bifurcation diagram depicted in Fig. 14.

In Fig. 16 another zoom of the preceding bifurcation diagram is shown which is similar to the bifurcation diagram of the Generalized Duffing oscillator. In this picture we can clearly see the process of period doubling, the emergence of chaotic motion and also small regular windows embedded inside the chaotic region. At the end of the chaotic region periodic oscillation occurs again with one more maximum. The same pattern repeats itself again and again, which we can observe from the zoom in Fig. 16, a typical snapshot appearing at a different scale during the whole bifurcation diagram until the amplitude is high enough and only a period-one attractor exists. For this segment we also plot the Lyapunov exponents, WADV and different recurrence quantifiers (DIV, L—mean diagonal line length, LAM—laminarity—percentage of recurrence points which form vertical lines, ENTR—Shannon entropy of diagonal line length distribution, V ENTROPY).

In Fig. 17 we show four different attractors, which are present for specific values of the parameters together with the map of basins of attraction. On the map, the complicated structure of the boundary between two basins is shown, which is visible also in the zoom of the map.

6. Concluding remarks

The aim of the paper is to highlight the fact that there are many interesting physical systems that cannot be adequately described by the classical approach wherein one prescribes constitutive relations for the forces acting in the components of a lumped parameter system in terms of the kinematics. While one can generalize the notion of what is meant by a solution to study some of these problems that are not amenable to a proper description by the classical approach, there are other problems which cannot be studied even within the context of the approaches used by

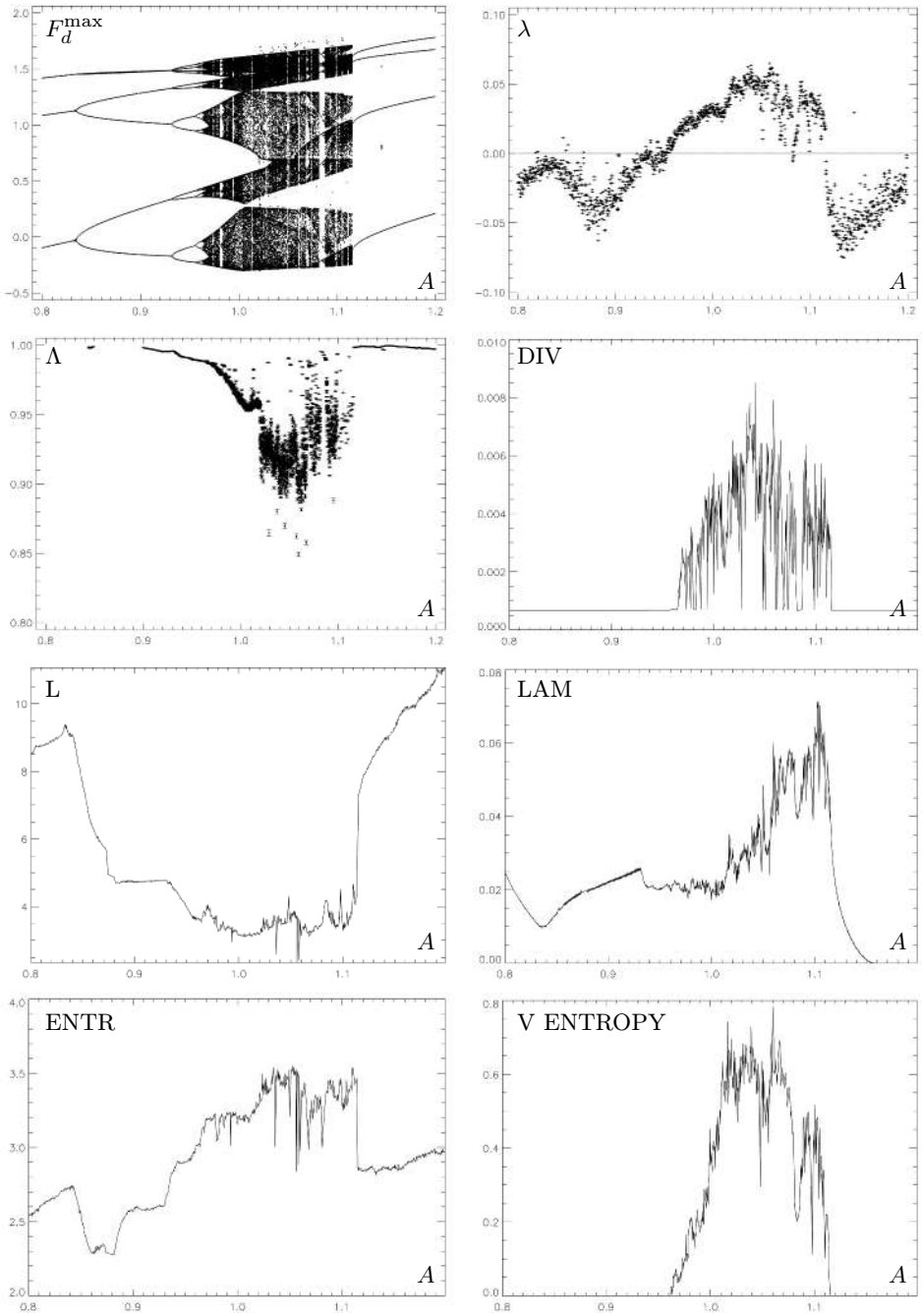

Figure 16. Bingham fluid: $\alpha = 0.6$, $\beta = 1.5$, $\delta = 0.7$, $\omega = 1.0$, another zoom of the same bifurcation diagram as in the previous picture and the corresponding WADV and recurrence quantifiers.

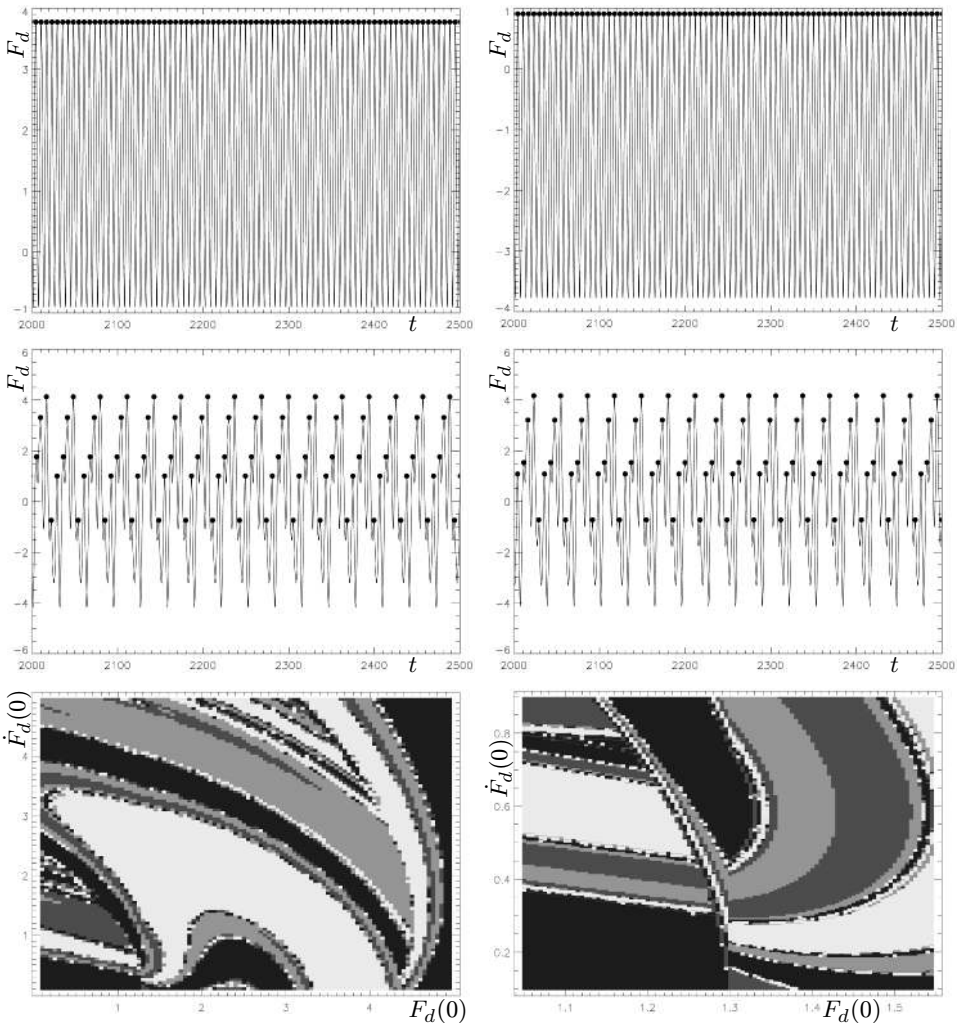

Figure 17. Bingham fluid: $\alpha = 1.1$, $\beta = 1.9$, $\delta = 1.3$, $\omega = 1.0$, $A = 2.37$, four different attractors existing for the same parameters and the map of basins of attraction, where each shade of grey corresponds to one of the attractors.

Filippov. When working with nonlinear problems, one might be able to adapt ideas introduced by Colombeau [5], [6] and Rosinger [19], [20] concerning a generalization of the theory of distributions. One should prefer to work with the original system (1.1), (1.6) and avoid transferring the problem to a higher order equation either for x or F_s. We indicated that chaotic behavior of the system that is usually, within the context considered in this study, associated with the original Duffing oscillator (see [15]) with $\beta_D < 0$, can be observed for the physically relevant problems such as

damped rigid-elastic spring or the Bingham dashpot with a linear spring. Chaotic behavior is a consequence of the constraints involved in the model descriptions that make the problem nonlinear.

Even the staid field of the vibration of lumped parameter systems provides challenging problems in mathematical analysis and interesting new physical insight.

References

[1] *J.-P. Aubin, A. Cellina*: Differential Inclusions. Set-Valued Maps and Viability Theory. Grundlehren der Mathematischen Wissenschaften 264, Springer, Berlin, 1984.

[2] *M. Bulíček, P. Gwiazda, J. Málek, K. R. Rajagopal, A. Świerczewska-Gwiazda*: On flows of fluids described by an implicit constitutive equation characterized by a maximal monotone graph. Mathematical Aspects of Fluid Mechanics. Selected Papers Based on the Presentations at the Workshop Partial Differential Equations and Fluid Mechanics, Warwick, 2010 (J. C. Robinson et al., eds.). London Math. Soc. Lecture Note Ser. 402, Cambridge University Press, Cambridge, 2012, pp. 23–51.

[3] *M. Bulíček, P. Gwiazda, J. Málek, A. Świerczewska-Gwiazda*: On unsteady flows of implicitly constituted incompressible fluids. SIAM J. Math. Anal. *44* (2012), 2756–2801.

[4] *M. Bulíček, J. Málek, K. R. Rajagopal*: On Kelvin-Voigt model and its generalizations. Evol. Equ. Control Theory (electronic only) *1* (2012), 17–42.

[5] *J.-F. Colombeau*: New Generalized Functions and Multiplication of Distributions. North-Holland Mathematics Studies 84, North-Holland Publishing, Amsterdam, 1984.

[6] *J.-F. Colombeau*: Multiplication of Distributions. A Tool in Mathematics, Numerical Engineering and Theoretical Physics. Lecture Notes in Mathematics 1532, Springer, Berlin, 1992.

[7] *K. Deimling*: Multivalued Differential Equations. De Gruyter Series in Nonlinear Analysis and Applications 1, Walter de Gruyter, Berlin, 1992.

[8] *J.-P. Eckmann, S. Oliffson Kamphorst, D. Ruelle*: Recurrence plots of dynamical systems. Europhys. Lett. *4* (1987), 973–977.

[9] *A. F. Filippov*: Classical solutions of differential equations with multi-valued right-hand side. SIAM J. Control *5* (1967), 609–621.

[10] *A. F. Filippov*: Differential Equations with Discontinuous Righthand Sides (F. M. Arscott, ed.). Mathematics and Its Applications: Soviet Series 18, Kluwer Academic Publishers, Dordrecht, 1988.

[11] *D. T. Kaplan, L. Glass*: Direct test for determinism in a time series. Phys. Rev. Lett. *68* (1992), 427–430.

[12] *O. Kopáček, V. Karas, J. Kovář, Z. Stuchlík*: Transition from regular to chaotic circulation in magnetized coronae near compact objects. Astrophys. J. *722* (2010), 1240–1259.

[13] *N. Marwan, M. C. Romano, M. Thiel, J. Kurths*: Recurrence plots for the analysis of complex systems. Phys. Rep. *438* (2007), 237–329.

[14] *L. Meirovitch*: Elements of Vibration Analysis. McGraw-Hill Book Company, Düsseldorf, 1975.

[15] *E. Ott*: Chaos in Dynamical Systems. Cambridge University Press, Cambridge, 2002.

[16] *D. Pražák*: Remarks on the uniqueness of second order ODEs. Appl. Math., Praha *56* (2011), 161–172.

[17] *D. Pražák, K. R. Rajagopal*: Mechanical oscillators described by a system of differential-algebraic equations. Appl. Math., Praha *57* (2012), 129–142.

[18] *K. R. Rajagopal*: A generalized framework for studying the vibrations of lumped parameter systems. Mech. Res. Commun. *37* (2010), 463–466.

[19] *E. E. Rosinger*: Generalized Solutions of Nonlinear Partial Differential Equations. North-Holland Mathematics Studies 146, North-Holland Publishing, Amsterdam, 1987.
[20] *E. E. Rosinger*: Nonlinear Partial Differential Equations. An Algebraic View of Generalized Solutions. North-Holland Mathematics Studies 164, North-Holland, Amsterdam, 1990.
[21] *O. Semerák, P. Suková*: Free motion around black holes with discs or rings: between integrability and chaos–II. Mon. Not. R. Astron. Soc. *425* (2012), 2455–2476.
[22] *D. E. Stewart*: Rigid-body dynamics with friction and impact. SIAM Rev. *42* (2000), 3–39.
[23] *P. Suková*: Chaotic geodesic motion around a black hole and disc. J. Phys. Conf. Ser. *314* (2011), Article ID 012087.
[24] *P. Suková, O. Semerák*: Recurrence of geodesics in a black-hole-disc field. AIP Conference Proceedings *1458* (2012), 523–526.
[25] *P. Suková, O. Semerák*: Free motion around black holes with discs or rings: between integrability and chaos–III. Mon. Not. R. Astron. Soc. *436* (2013), 978–996.
[26] *Y. Ueda*: Randomly transitional phenomena in the system governed by Duffing's equation. J. Stat. Phys. *20* (1979), 181–196.
[27] *K. Zaki, S. Noah, K. R. Rajagopal, A. R. Srinivasa*: Effect of nonlinear stiffness on the motion of a flexible pendulum. Nonlinear Dyn. *27* (2002), 1–18.
[28] `http://www.recurrence-plot.tk/`.

Authors' addresses: *Josef Málek*, Mathematical Institute, Faculty of Mathematics and Physics, Charles University, Sokolovská 83, CZ-186 75 Praha 8, Czech Republic, e-mail: `malek@karlin.mff.cuni.cz`; *Petra Suková*, Center for Theoretical Physics, Polish Academy of Sciences, Al. Lotnikow 32/46, 02-668 Warsaw, Poland, e-mail: `psukova@cft.edu.pl`; *Kumbakonam Ramamani Rajagopal*, Texas A&M University, College Station, TX 77840, Texas, United States of America, e-mail: `krajagopal@tamu.edu`.